



Effect of the intermediate principal stress on the mechanical responses of binary granular mixtures with different fines contents

Xiaoping Cao¹ · Yangui Zhu² · Jian Gong²

Received: 24 June 2020 / Accepted: 4 March 2021 / Published online: 29 March 2021
© The Author(s), under exclusive licence to Springer-Verlag GmbH Germany, part of Springer Nature 2021

Abstract

The effect of the intermediate principal stress (b quantifies its relative magnitude) on macroscale and microscale shear responses of binary granular mixtures with different fines contents (FCs) was investigated using the discrete element method. Mixtures were made up of coarse particles with real gravel shapes and fine particles with sphere shapes. True triaxial compression tests were conducted on their dense specimens. The shapes of coarse particles play an important role in the peak and critical friction angles and the peak dilatancy angles of binary granular mixtures. For mixtures with different FCs and an identical b , there is a linear relationship between the peak friction angle (or peak dilatancy angle) and the change in the void ratio. An acceptable equation was proposed to predict the peak dilatancy angle of a mixture. When $b = 0.2$ and 0.4 , the coaxiality of strain increments and stresses is affected by the FC. A previous study classified mixtures as “underfilled”, “interactive-underfilled”, “interactive-overfilled” and “overfilled” based on the percentage contributions of coarse–coarse, coarse–fine and fine–fine contacts to the shear strength. This study shows that the b value has little effect on the classification of mixtures at the peak and critical states. Furthermore, it was observed that there is a linear relationship between the relative peak dilatancy angle and the difference between the partial coordination numbers based on the “subsphere–subsphere” approach at the peak and critical states.

Keywords Binary granular mixtures · Intermediate principal stress · Contact types · Macroscale responses · Microscale responses

1 Introduction

The shear strength of a soil is influenced by the particle size distribution, particle shape, water content, direction of principal stresses, intermediate principal stress and so forth. When a slope is excavated, the soil is often subjected to three various principal stresses. Hollow cylinder torsion tests and true triaxial compression tests can be used to measure the shear responses of the soil in a three-dimensional stress

state. A parameter is often employed to quantify the relative magnitude of the intermediate principal stress. The parameter is defined as:

$$b = (\sigma_2 - \sigma_3) / (\sigma_1 - \sigma_3) \quad (1)$$

where σ_1 , σ_2 and σ_3 are the major, intermediate and minor principal stresses, respectively. Some experimental studies [1–6] were centered on the effect of the b value on the shear responses of soils. These studies indicated that both the peak and critical friction angles first increase and then decrease as the b value increases. However, these experimental studies mainly focused on the macroscale mechanical responses rather than the microscale mechanical responses. The discrete element method (DEM) is a good method for obtaining the macroscale and microscale mechanical responses of granular materials [7–9]. Many investigators [10–18] have employed the DEM to numerically investigate the effect of the b value on the shear responses of granular materials. In these numerical studies, the microscale mechanical responses, including the coordination number,

✉ Yangui Zhu
zyg19910707@csu.edu.cn

Xiaoping Cao
caoxp@mail.lzjtu.cn

Jian Gong
gj2018@csu.edu.cn

¹ School of Civil Engineering, Lanzhou Jiaotong University, Lanzhou 730070, China

² School of Civil Engineering, Central South University, Changsha 410075, China

sliding contacts, principal fabrics, particle rotations, and geometrical and mechanical anisotropies, were examined. However, the object of these numerical studies is the granular materials with narrow particle size distributions rather than the binary granular mixtures with wide particle size distributions.

Some natural slopes are composed of binary granular mixtures. The coarse particles and fine particles are the two components of binary granular mixtures. The coarse particles can be rocks, gravels and sands, and the fine particles can be sands, silts and clays [19–21]. The properties of binary granular mixtures are more complex than those of ordinary homogeneous geotechnical materials because of the nature of two components. Therefore, it is particularly important to investigate binary granular mixtures. Although some researchers [19–26] have studied binary granular mixtures, few studies have been conducted on the effect of the b value on the macroscale and microscale mechanical responses of binary granular mixtures via the DEM. The contacts in a binary granular mixture can be categorized as coarse–coarse (cc), coarse–fine (cf) and fine–fine (ff) contacts. According to the percentage contributions of the three contact types to the shear strength, three thresholds of the fine content (FC) were used to classify binary granular mixtures as four types, i.e., “underfilled”, “interactive-underfilled”, “interactive-overfilled”, and “overfilled” [27]. Note that the terms “underfilled” and “overfilled” used in dam engineering [28] were used. However, it is not clear whether the b value affects the classification of binary granular mixtures. In addition, the mechanisms by which the b value

affects the macroscale shear behaviors of binary granular mixtures with different FCs are not clear. Based on the above considerations, numerical simulations about the effect of the b value on the shear responses of binary granular mixtures were performed using the DEM in this study.

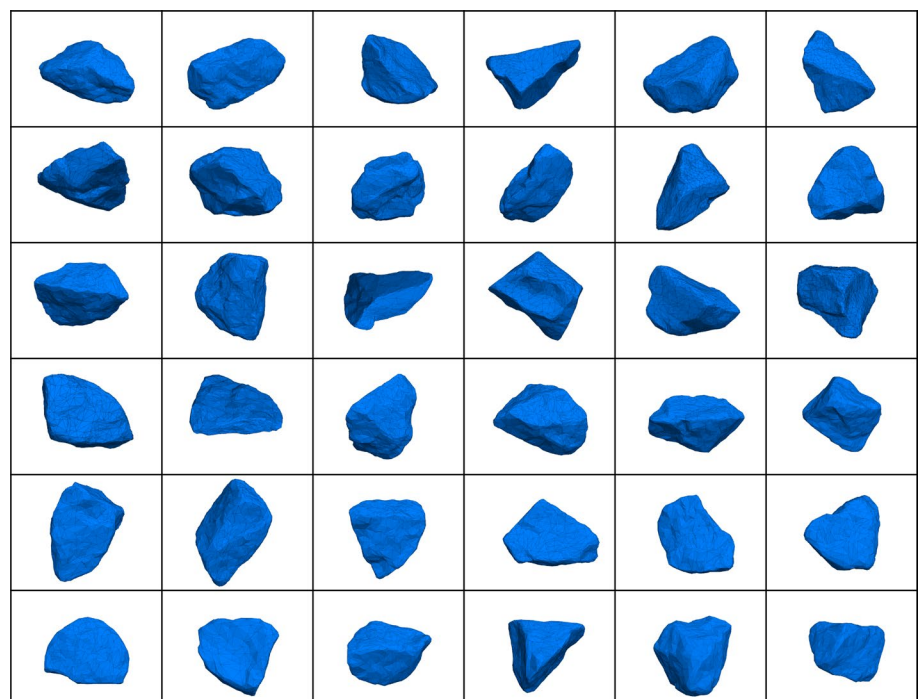
The main aim of this study is to systemically analyze the effect of the intermediate principal stress on the shear responses of binary granular mixtures with different FCs. Many true triaxial compression tests were performed on binary granular mixtures via the DEM. This work was arranged as follows. First, the numerical simulation process was presented. Then, the macroscale responses, contributions of contact types, microscale responses, and anisotropies of contacts and contact forces were examined. Lastly, some main conclusions were obtained.

2 Numerical simulation process

2.1 Coarse and fine particles

Binary granular mixtures were composed of coarse and fine particles. In this study, the coarse and fine particles can be viewed as gravels and sands, respectively. The geometries of coarse particles can be obtained by scanning real gravels with a three-dimensional scanner called Wiiboox Reeyee. The scan file for each gravel is a file suffixed by stl. 36 gravels with various shapes were scanned, and their scan images are shown in Fig. 1. Each scan image has 1500 triangular meshes. Then, the scan files were imported into PFC^{3D} [29],

Fig. 1 Scan images of 36 differently shaped gravels



and the geometries of the gravels were filled with overlapping subspheres [30]. Accordingly, these multisphere particles approximately replaced coarse particles. The number of subspheres of each coarse particle is 168–362. In reality, some sands are round in shape, such as Ottawa sands [31–33]. In addition, the use of spherical fine particles can significantly improve the computational efficiency. Based on the two facts, the fine particles were treated as spherical particles in this study. Note that all particles are unbreakable. The volume of a coarse particle is equal to that of a sphere with a diameter of 15 mm, and the diameter of a fine particle is 3.37 mm. Accordingly, a particle size ratio of 4.45 was used in this study, consistent with that of Lopez et al. [27, 34]. Lade et al. [35] and Shire et al. [36] found a phenomenon. The minimum void ratio of a binary granular mixture (FC \approx 30%) decreases sharply in the beginning as the particle size ratio increases. When the particle size ratio is beyond 6.5, the effect of the particle size ratio on the minimum void ratio is much less pronounced. Thus, the behaviors of binary granular mixtures can be expected to change as the particle size ratio exceeds 6.5. The FC ranges from 0 to 100% in intervals of 10%. Before the specimen generation, the number of coarse particles was given. Accordingly, the number of fine particles could be determined according to the FC. For all binary granular mixtures, the numbers of coarse and fine particles are shown in Table 1.

2.2 Specimen generation

The DEM program PFC^{3D} [29] was employed to execute the numerical true triaxial compression tests. The linear contact model was employed to describe the inter-particle and wall-particle interactions. Table 2 provides the parameters of the linear contact model. Horn and Deere [37] discovered that the friction coefficient of saturated quartz

Table 2 Parameters of the linear contact model

Parameter	Value
Particle density (kg/m ³)	2600
Inter-particle friction coefficient during the specimen generation	0
Inter-particle friction coefficient during the true triaxial compression	0.5
Wall-particle friction coefficient	0
Effective modulus (Pa)	1.0×10^8
Normal-to-tangential stiffness ratio	4/3
Damping factor	0.7

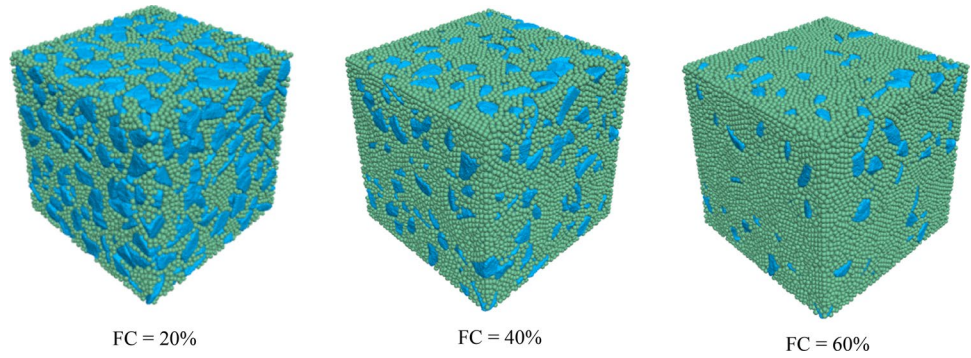
particles is 0.42–0.45. Rowe [38] found that the friction coefficient of saturated quartz particles is 0.40–0.60. Senetakis et al. [39, 40] discovered that the friction coefficient of saturated quartz particles is 0.12–0.35. In this study, the inter-particle friction coefficient during the test was set to 0.5, identical with that used by Guo and Zhao [41, 42], Gu et al. [43] and Gong et al. [24]. Coetzee [44] calibrated the effective modulus of the contacts between crushed rock particles as 0.38×10^8 Pa to 1.14×10^8 Pa using PFC^{3D}. In this study, the effective modulus was set to 1.0×10^8 Pa, identical with that used by Gong et al. [24] and approximate to that used by Guo and Zhao [41, 42] and Gu et al. [43]. Goldenberg and Goldhirsch [45] deemed that the normal-to-tangential stiffness ratio should be in the range of (1.0, 1.5) for real granular materials. In this study, the normal-to-tangential stiffness ratio was set to 4/3. Jiang et al. [46] pointed out that the damping factor has no significant effect on a quasi-static test and selected its value as 0.7 by trial and error. In this study, the damping factor was set to 0.7, identical with that used by Gu et al. [43] and Gong et al. [24].

First, all particles without overlap were stochastically distributed in a large cube area formed by six rigid walls. To obtain isotropically dense specimens, the gravitational acceleration and the inter-particle and wall-particle friction coefficients were temporarily remained at zero. Then, the walls and particles were moved inward. To stop particles from exiting the cube area, all particles were calmed every 10 steps until 20,000 steps. Subsequently, a servo-control mechanism was employed to isotropically compress all particles. Finally, if the ratio of the average unbalanced force to the average contact force was smaller than 1.0×10^{-4} and the deviation of the wall stress from 200 kPa was smaller than 1 kPa, the specimen equilibrated. Frictionless particles were used, thus all specimens had a relative density of 100%, in line with Lopez et al. [27, 34]. The dimensions and initial porosities of all specimens before shear are also included in Table 1. Figure 2 presents the specimens of binary granular mixtures with FC = 20%, 40% and 60% before shear.

Table 1 Basic information of the specimens

FC (%)	Dimensions (mm)	The number of coarse particles	The number of fine particles	The initial porosity
0	138 × 136 × 137	1000	0	0.350
10	132 × 132 × 133	876	8139	0.297
20	130 × 131 × 130	771	16,117	0.274
30	131 × 130 × 130	676	24,226	0.269
40	131 × 131 × 132	579	32,278	0.286
50	132 × 132 × 132	482	40,306	0.299
60	133 × 133 × 133	384	48,169	0.311
70	133 × 133 × 134	288	56,224	0.324
80	134 × 133 × 135	191	63,937	0.337
90	135 × 134 × 135	95	71,554	0.350
100	43 × 43 × 44	0	2500	0.391

Fig. 2 Specimens of binary granular mixtures with FC=20%, 40% and 60% before shear



2.3 True triaxial compression

When the specimen generation was completed, the inter-particle friction coefficient was adjusted to 0.5 and the wall-particle friction coefficient was remained at zero. In drained true triaxial compression tests, σ_1 was changed by shifting the top wall down at an invariable velocity and σ_3 was maintained at 200 kPa by a servo-control mechanism. σ_2 varied with σ_1 by a servo-control mechanism, meanwhile, the b value remained constant. In this study, $b=0, 0.2, 0.4, 0.6, 0.8$ and 1. The loading rate should be small enough to make tests quasi-static. This can be described by the inertia parameter I [47], which should be less than 2.5×10^{-3} [48], as follows:

$$I = \frac{d\varepsilon_1}{dt} d \sqrt{\rho/\sigma_3} \tag{2}$$

where $\frac{d\varepsilon_1}{dt}$ denotes the axial strain rate, d denotes the mean of the diameters of all particles, and ρ denotes the particle density. The loading rate of the top wall was set to 0.05 m/s, therefore I was smaller than 1.0×10^{-3} in this study. Following Zhou et al. [18], the true triaxial compression tests were terminated when the axial strain ε_1 reached 40%.

3 Analyses of simulation results

3.1 Macroscale responses

Using the microscale quantities in an entire specimen, the stress tensor σ_{ij} is determined by [49]:

$$\sigma_{ij} = \frac{1}{V} \sum_{c=1}^C f_i^c d_j^c \tag{3}$$

where V denotes the volume of the specimen, C denotes the number of contacts, and f_i^c and d_j^c denote the i th component of the contact force and the j th component of the branch vector at contact c , respectively. The average stress p and the deviatoric stress q are defined as:

$$p = \sigma_{ii}/3 \tag{4}$$

$$q = \sqrt{\frac{3}{2} \sigma'_{ij} \sigma'_{ij}} \tag{5}$$

where σ'_{ij} denotes the deviatoric part of σ_{ij} . In this study, the friction angle ϕ of binary granular mixtures is calculated by:

$$\sin \phi = \frac{\sigma_1 - \sigma_3}{\sigma_1 + \sigma_3} = \frac{(q/p) \cdot 1 / (1 - b + b^2)^{0.5}}{2 + (q/p) \cdot (1/3 - 2b/3) / (1 - b + b^2)^{0.5}} \tag{6}$$

The axial strain ε_1 , the lateral strains ε_2 and ε_3 , the volumetric strain ε_v , and the deviatoric strain ε_d are given by:

$$\varepsilon_1 = (L_{1,0} - L_1) / L_{1,0} \tag{7a}$$

$$\varepsilon_2 = (L_{2,0} - L_2) / L_{2,0} \tag{7b}$$

$$\varepsilon_3 = (L_{3,0} - L_3) / L_{3,0} \tag{7c}$$

$$\varepsilon_v = (V_0 - V) / V_0 \tag{8}$$

$$\varepsilon_d = \frac{\sqrt{2}}{3} \sqrt{(\varepsilon_1 - \varepsilon_2)^2 + (\varepsilon_2 - \varepsilon_3)^2 + (\varepsilon_3 - \varepsilon_1)^2} \tag{9}$$

where $L_{1,0}$, $L_{2,0}$ and $L_{3,0}$ are the dimensions of the specimen before shear, respectively; L_1 , L_2 and L_3 are the dimensions of the specimen during the test, respectively; V_0 and V are the volumes of the specimen before shear and during the test, respectively. The dilatancy angle ψ is given by [50]:

$$\sin \psi = - \frac{d\varepsilon_v / d\varepsilon_1}{2 - d\varepsilon_v / d\varepsilon_1} \tag{10}$$

To study the size effect, three specimens (FC = 30%) with different sizes were prepared and tested ($b=0$). The dimensions of three specimens are $131 \times 130 \times 130$ mm, $164 \times 163 \times 163$ mm and $206 \times 205 \times 206$ mm, respectively. Namely, the ratios of the minimum specimen size to the maximum particle size are 8.7, 10.9 and 13.7, respectively.

The computational efficiency of the largest specimen is extremely low, therefore the largest specimen was not compressed to the axial strain of 40%. Figure 3 shows the evolutions of the stress ratio q/p and volumetric strain ε_v versus the axial strain ε_1 for the specimens with different sizes when $FC = 30\%$ and $b = 0$. Clearly, the specimen size has a slight effect on $q/p - \varepsilon_1$ and $\varepsilon_v - \varepsilon_1$ relationships of binary granular mixtures. Nie et al. [51] found that the specimen size has a slight effect on $q/p - \varepsilon_1$ and $\varepsilon_v - \varepsilon_1$ relationships when the ratio of the minimum specimen size to the maximum particle size ranges from about 10 to about 20. Hence, it is reasonable to use the smallest specimen ($131 \times 130 \times 130$ mm) to improve the computational efficiency. To exclude the specimen size effect, Jamiolkowski et al. [52] suggested that the ratio of the minimum specimen size to the maximum particle size should be at least 5 and that the ideal ratio was 8. ASTM suggested that the ratio should not be less than 6. The industry standard of China: Code for Soil Test of Railway Engineering (TB 10102-2010, J 1135-2010) suggested that

the ratio should not be less than 5. In this paper, the ratios of all specimens are larger than 8.5. Based on the above numerical simulation results and those recommendations for laboratory tests, it can be concluded that the size effect in this study is very limited. In future work, the numerical simulations of much larger specimens are needed to further confirm the size effect.

Figure 4 presents the evolutions of the stress ratio q/p with the axial strain ε_1 for binary granular mixtures with $FC = 10\%$ and $FC = 50\%$. With increasing ε_1 , q/p increases rapidly to a crest and then slowly decreases to a basically steady value. Additionally, the b value affects q/p ; that is, q/p generally decreases with an increase in the b value. Figure 5 illustrates the variations in the stress ratio q/p with the FC at the peak and critical states. As shown in Fig. 5a, with increasing FC, q/p gradually decreases to a basically steady value; with increasing b , q/p generally decreases. The variation trends of the curves in Fig. 5b basically resemble those in Fig. 5a. Using Eq. (6), the peak

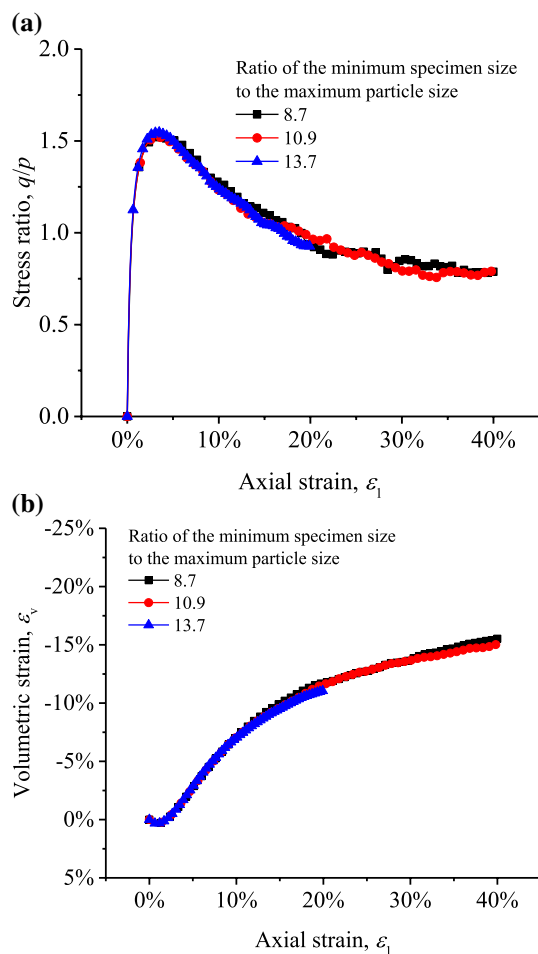


Fig. 3 Evolutions of the **a** stress ratio and **b** volumetric strain versus the axial strain for the specimens with different sizes when $FC = 30\%$ and $b = 0$

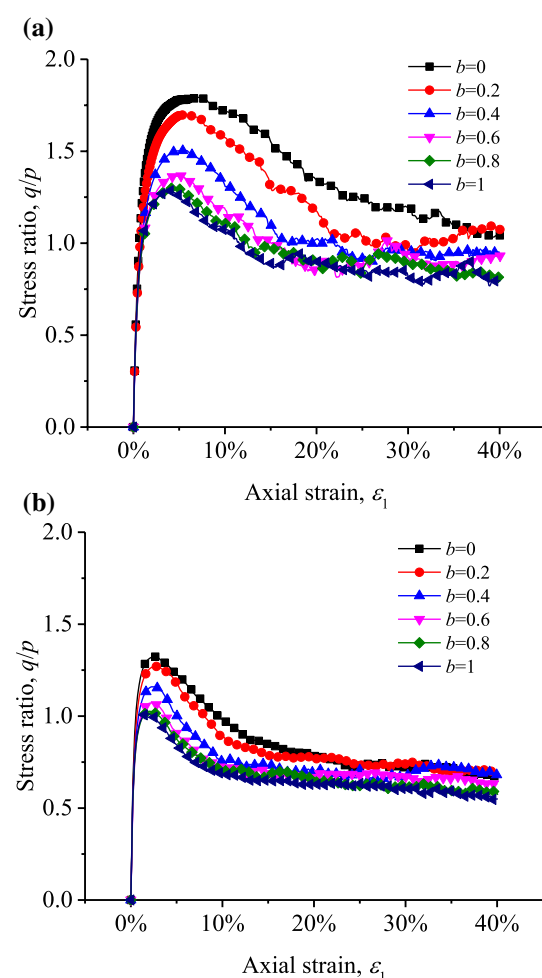


Fig. 4 Evolutions of the stress ratio with the axial strain for binary granular mixtures with **a** $FC = 10\%$ and **b** $FC = 50\%$

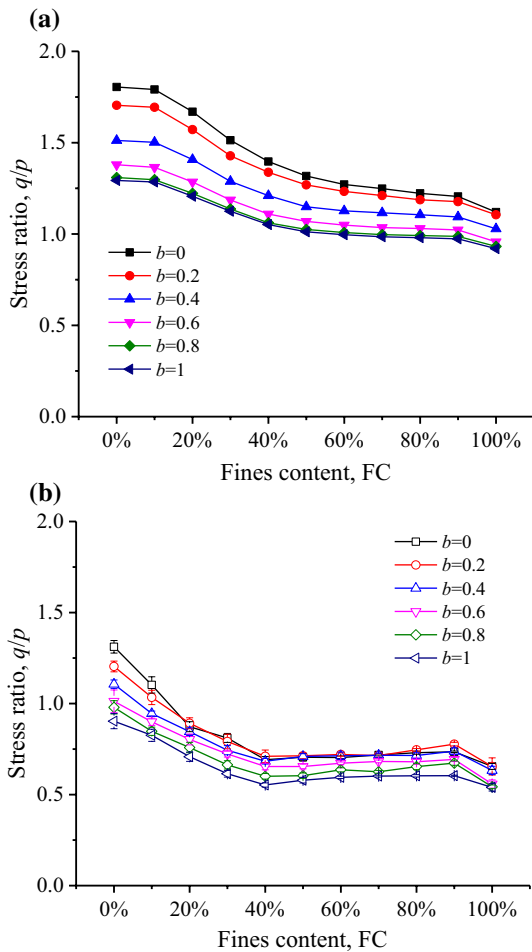


Fig. 5 Variations in the stress ratio with the FC at the **a** peak and **b** critical states

friction angle ϕ_p and the critical friction angle ϕ_c were calculated, as shown in Fig. 6. In Fig. 6a, for a specific FC, as the b value increases, ϕ_p first increases to a crest and then decreases. For a specific b , when $FC \leq 40\%$, ϕ_p decreases with increasing FC; when $FC \geq 50\%$, ϕ_p varies within a very small range. The variation trends of ϕ_c with respect to the b value and the FC in Fig. 6b are roughly similar to those of ϕ_p in Fig. 6a. O’Sullivan et al. [13] used a simple buckling model to explain why the b value influences the friction angles of granular materials. When the b value changes, there is a change in the lateral support provided by the force chains along the directions of intermediate and minor principal stresses; the change in the lateral support directly influences the buckling of strong force chains along the direction of the major principal stress. For a binary granular mixture with a specific FC and a specific shear state, with increasing b , the maximum and minimum friction angles (i.e., ϕ_{max} and ϕ_{min}) were observed. Note that ϕ_{min} always occurs at $b=0$, whereas ϕ_{max} always occurs at $b=0.4$ or $b=0.6$.

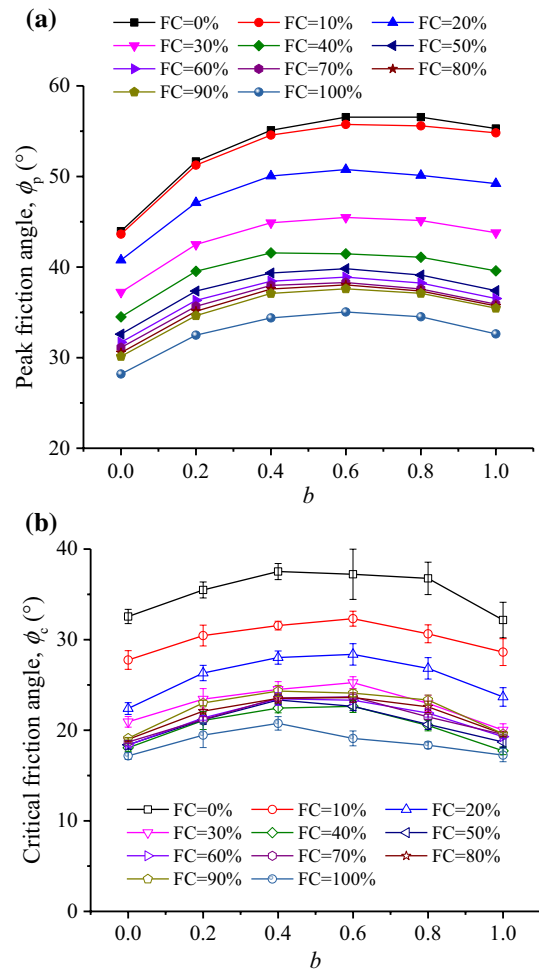


Fig. 6 Variations in the **a** peak and **b** critical friction angles with the b value

To compare the mechanical responses of the binary granular mixtures with different coarse particle shapes, additional numerical simulations were performed on the binary granular mixtures ($FC = 0\%, 10\%, 20\%, 30\%, 40\%, 60\%, 80\%$ and 100%) with spherical coarse particles. For the sake of conciseness, Fig. 7a presents the variation in the friction angle versus the FC when $b=0.4$. For mixtures with real gravel-shaped coarse particles, with increasing FC, both ϕ_p and ϕ_c gradually decreases to a generally steady value. For mixtures with spherical coarse particles, ϕ_p shows its maximum at $FC = 30\%$, whereas the FC has a negligible effect on ϕ_c . Additionally, when $FC \leq 40\%$, for a given FC, the friction angle of a mixture with real gravel-shaped coarse particles is clearly larger than that of a mixture with spherical coarse particles. Figure 7b presents the variation in the difference between the maximum and minimum friction angles $\phi_{max} - \phi_{min}$ versus the FC with increasing b . For mixtures with real gravel-shaped coarse particles, when $FC \leq 40\%$, as the FC increases, $\phi_{p,max} - \phi_{p,min}$ ($\phi_{max} - \phi_{min}$

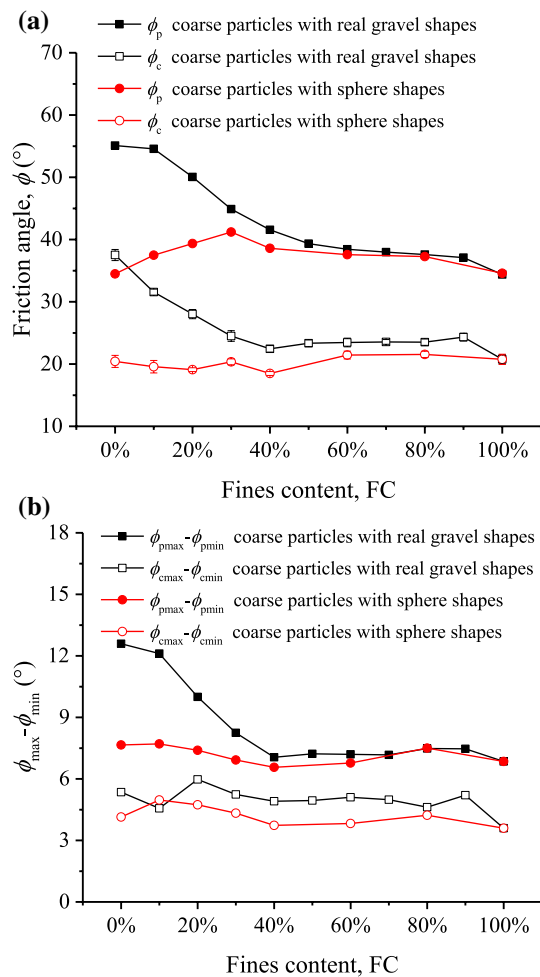


Fig. 7 a Variation in the friction angle versus the FC when $b=0.4$; b variation in the difference between the maximum and minimum friction angles versus the FC with increasing b

at the peak state) gradually decreases; when $FC \geq 40\%$, as the FC increases, $\phi_{p\max} - \phi_{p\min}$ is generally stable. For mixtures with spherical coarse particles, the FC has a negligible effect on $\phi_{p\max} - \phi_{p\min}$. Regardless of the shapes of coarse particles, the FC has a negligible effect on $\phi_{c\max} - \phi_{c\min}$ ($\phi_{\max} - \phi_{\min}$ at the critical state). In addition, for a given FC, $\phi_{p\max} - \phi_{p\min}$ is larger than $\phi_{c\max} - \phi_{c\min}$. Figure 7 indicates that the shapes of coarse particles play an important role in the peak and critical friction angles of binary granular mixtures.

Figure 8 presents the evolutions of the volumetric strain ε_v versus the axial strain ε_1 for binary granular mixtures with $FC = 10\%$ and $FC = 50\%$. With increasing ε_1 , the specimen initially contracts and then dilates. In the initial loading stage, the contraction of the specimen increases with increasing b . As the loading continues ($\varepsilon_1 \leq 20\%$ for $FC = 10\%$, $\varepsilon_1 \leq 10\%$ for $FC = 50\%$), the dilation of the specimen increases with increasing b . In the final loading

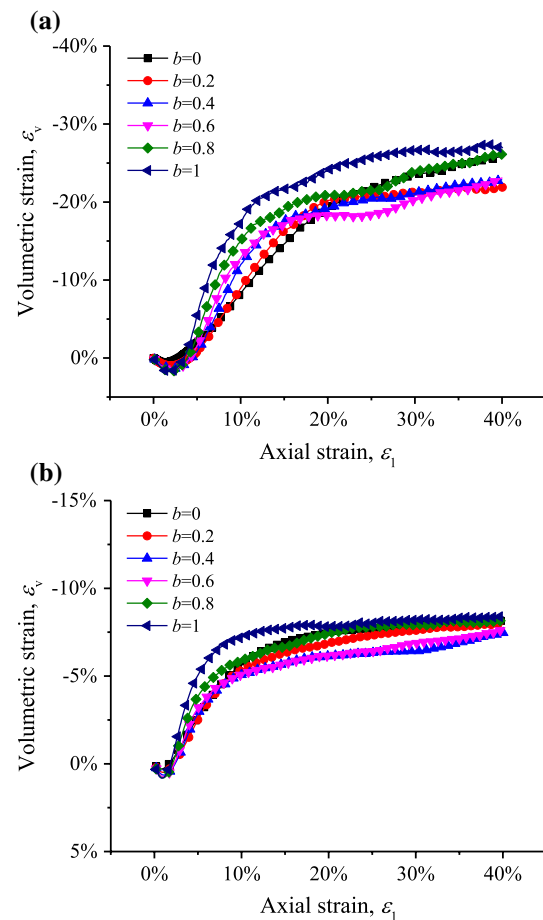


Fig. 8 Evolutions of the volumetric strain versus the axial strain for binary granular mixtures with a $FC = 10\%$ and b $FC = 50\%$

stage, the dilation of the specimen first decreases and then increases with increasing b . Figure 9 presents the evolution of the dilatancy angle ψ versus the axial strain ε_1 for the binary granular mixture with $FC = 50\%$. As ε_1 increases, ψ first increases to a crest and then decreases to a value close to zero. It was observed that the b value affects the peak dilatancy angle. Figure 10 shows the variation in the peak dilatancy angle ψ_p versus the b value. As the b value increases, ψ_p roughly linearly increases. For a given b value, the ψ_p values of the binary granular mixtures with $FC \leq 20\%$ are obviously larger than those of the binary granular mixtures with $FC \geq 30\%$. For a binary granular mixture with a specific FC, with increasing b , the maximum and minimum peak dilatancy angles (i.e., $\psi_{p\max}$ and $\psi_{p\min}$) were observed. Note that $\psi_{p\min}$ always occurs at $b=0$, whereas $\psi_{p\max}$ always occurs at $b=1$.

For the sake of conciseness, Fig. 11a presents the variation in the peak dilatancy angle versus the FC when $b=0.4$. For mixtures with real gravel-shaped coarse particles, the ψ_p values of mixtures with $FC \leq 20\%$ are obviously larger than those of mixtures with $FC \geq 30\%$. For mixtures

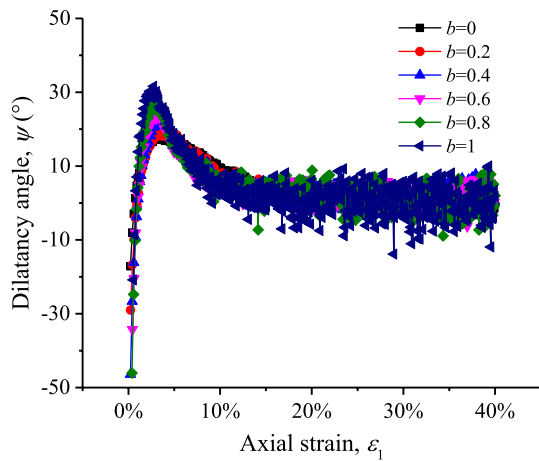


Fig. 9 Evolution of the dilatancy angle versus the axial strain for the binary granular mixture with FC=50%

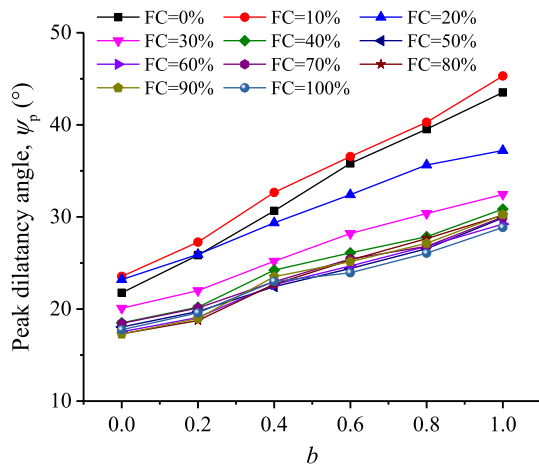


Fig. 10 Variation in the peak dilatancy angle versus the b value

with spherical coarse particles, ψ_p shows its maximum at FC = 30%. Additionally, when $FC \leq 20\%$, for a given FC, ψ_p of a mixture with real gravel-shaped coarse particles is clearly larger than that of a mixture with spherical coarse particles. Figure 11b presents the variation in the difference between the maximum and minimum peak dilatancy angles $\psi_{pmax} - \psi_{pmin}$ versus the FC with increasing b . For mixtures with real gravel-shaped coarse particles, when $FC \leq 30\%$, $\psi_{pmax} - \psi_{pmin}$ roughly decreases with increasing FC; with a further increase in the FC, there is no significant change in $\psi_{pmax} - \psi_{pmin}$. For mixtures with spherical coarse particles, the FC has a negligible effect on $\psi_{pmax} - \psi_{pmin}$. Figure 11 indicates that the shapes of coarse particles play an important role in the peak dilatancy angles of binary granular mixtures.

In this study, a concept called “change in the void ratio” $R_{vc} - R_{vi}$ was used, where R_{vc} and R_{vi} are the void ratios

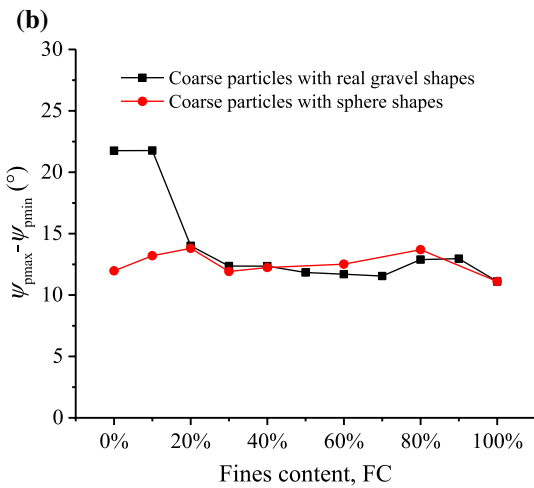
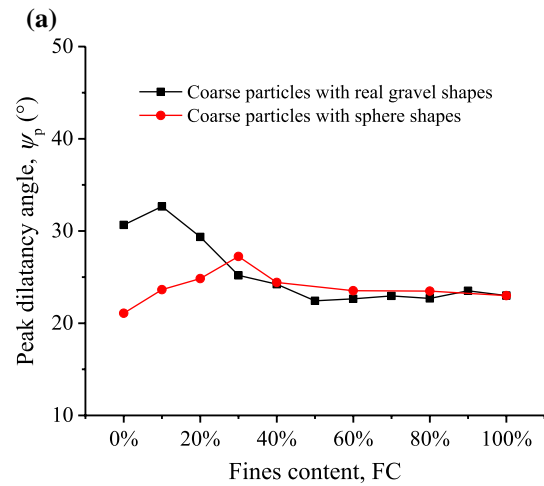


Fig. 11 **a** Variation in the peak dilatancy angle versus the FC when $b=0.4$; **b** variation in the difference between the maximum and minimum peak dilatancy angles versus the FC with increasing b

of a specimen at the critical and initial states, respectively. Figure 12a and b show the relationships between the change in the void ratio $R_{vc} - R_{vi}$ and the peak friction angle ϕ_p and the peak dilatancy angle ψ_p . Obviously, for a given b value, the data for binary granular mixtures with different FCs can be fitted by $\phi_p = m(R_{vc} - R_{vi}) + n$ or $\psi_p = k(R_{vc} - R_{vi}) + l$. This finding means that a larger $R_{vc} - R_{vi}$ will lead to a larger ϕ_p and ψ_p for a given b value. The insets show the variations in the slope and the intercept versus the b value. In the insets in Fig. 12a, with increasing b , m increases to a plateau and n initially increases and then decreases. In the insets in Fig. 12b, with increasing b , both k and l increase. These findings mean that the two linear relationships depend on the b value. Figure 12c shows the relationship between the change in the void ratio $R_{vc} - R_{vi}$ and the modified peak dilatancy angle $\psi_p/e^{0.52b}$. Obviously, the data can be fitted by $\psi_p/e^{0.52b} = 30.725(R_{vc} - R_{vi}) + 14.424$.

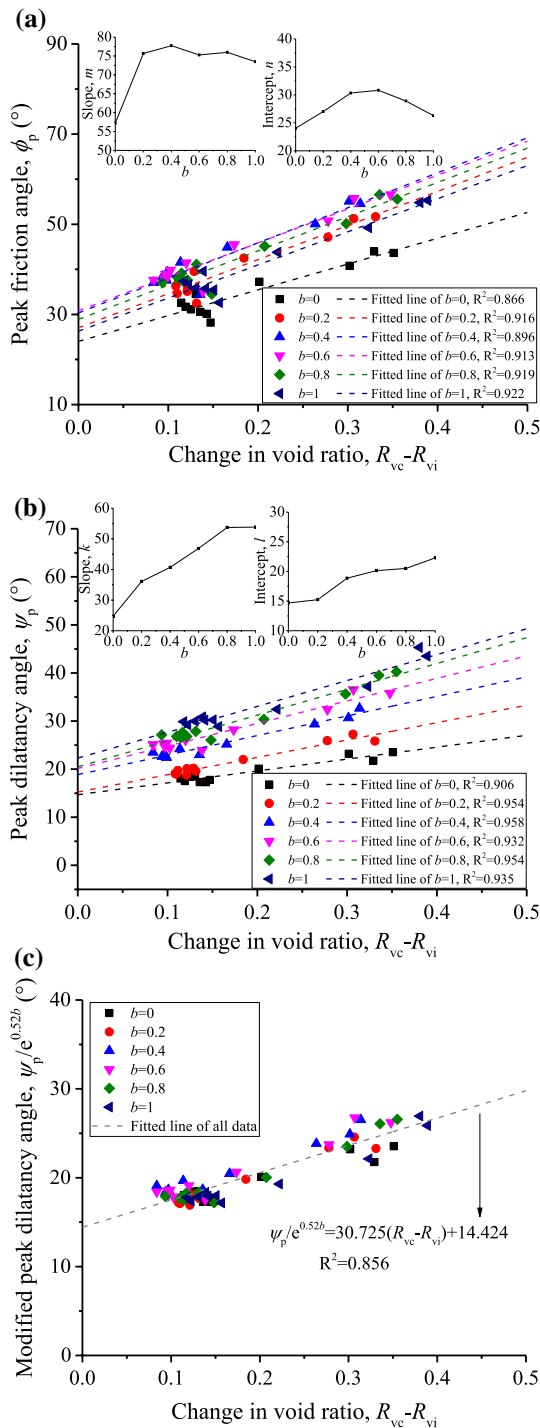


Fig. 12 Relationships between the change in the void ratio and the **a** peak friction angle, **b** peak dilatancy angle and **c** modified peak dilatancy angle

This finding indicates that the acceptable equation $\psi_p = e^{0.52b} [30.725(R_{vc} - R_{vi}) + 14.424]$ can be used to predict the peak dilatancy angle of a binary granular mixture with a given b value and a given FC.

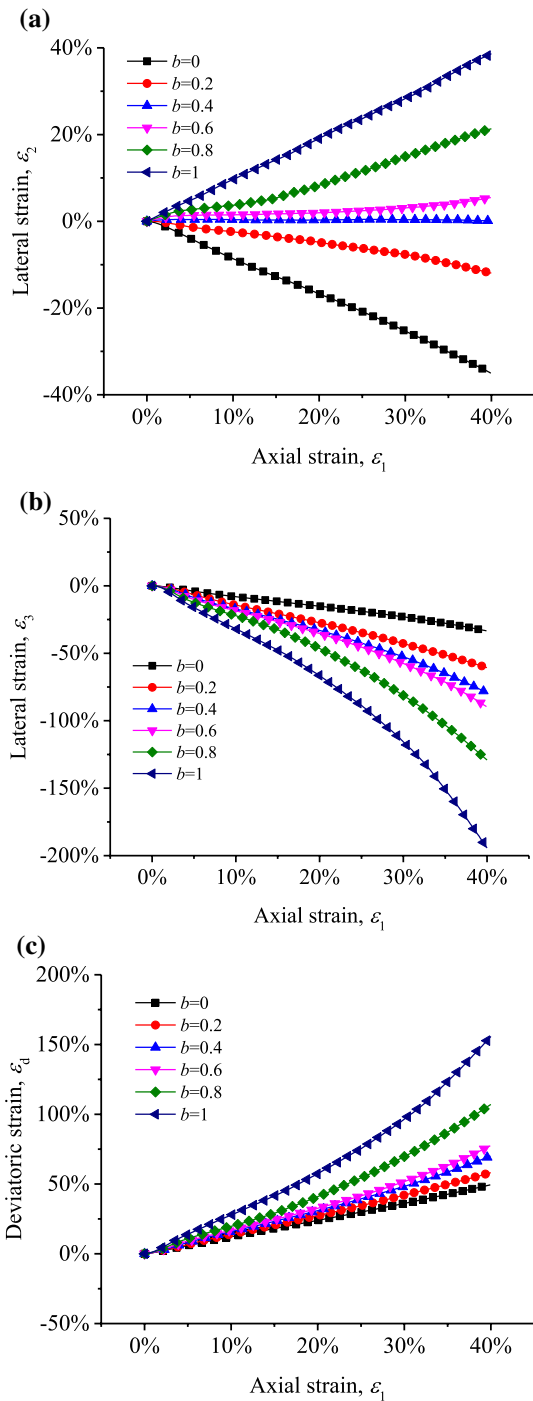


Fig. 13 Evolutions of the lateral strains and the deviatoric strain with the axial strain for the binary granular mixture with FC = 50%

Figure 13 presents the evolutions of the lateral strains (ϵ_2 and ϵ_3) and the deviatoric strain ϵ_d with the axial strain ϵ_1 for the binary granular mixture with FC = 50%. In Fig. 13a, when $b \leq 0.2$, ϵ_2 decreases with increasing ϵ_1 ; when $b = 0.4$, ϵ_2 generally remains at 0 with increasing ϵ_1 ; when $b \geq 0.6$, ϵ_2 increases with increasing ϵ_1 . Additionally, ϵ_2 increases

with an increase in the b value. In Fig. 13b, ϵ_3 decreases with increasing ϵ_1 ; ϵ_3 decreases with an increase in the b value. In Fig. 13c, ϵ_d increases with increasing ϵ_1 ; ϵ_d increases with increasing b . Zhao and Guo [53] and Zhou et al. [54] used a parameter to characterize the coaxiality of the contacts and stresses. Similarly, a parameter can be used to characterize the coaxiality of the strain increments and stresses. The coaxiality parameter can be defined as:

$$A = \frac{\text{tr}(\alpha'_{ij}\beta'_{ij})}{\sqrt{\alpha'_{ij}\alpha'_{ij}}\sqrt{\beta'_{ij}\beta'_{ij}}} \tag{11}$$

where α'_{ij} and β'_{ij} are the deviatoric tensors of α_{ij} and β_{ij} , respectively. The expressions of α_{ij} and β_{ij} are as follows:

$$\alpha_{ij} = \begin{bmatrix} d\epsilon_1 & & \\ & d\epsilon_2 & \\ & & d\epsilon_3 \end{bmatrix} \tag{12a}$$

$$\beta_{ij} = \begin{bmatrix} \sigma_1 & & \\ & \sigma_2 & \\ & & \sigma_3 \end{bmatrix} \tag{12b}$$

where $d\epsilon_1, d\epsilon_2$ and $d\epsilon_3$ are the strain increments corresponding to ϵ_1, ϵ_2 and ϵ_3 , respectively. Figure 14 presents the variations in the coaxiality parameter A with the FC at the peak and critical states. When $b=0$ and 1, $A \approx 1$, which means that the strain increments and the stresses are coaxial. For a specific FC, with increasing b , A first decreases and then increases, which means that an increase in b causes the coaxiality to first weaken and then strengthen. In Fig. 14a, for $b=0, 0.6, 0.8$ and 1, A hardly changes with increasing FC. For $b=0.2$ and 0.4, A increases with increasing FC. In Fig. 14b, for $b=0, 0.6, 0.8$ and 1, A remains roughly unchanged with increasing FC. For $b=0.2$, A first increases and then decreases with increasing FC. For $b=0.4$, A increases with increasing FC. These findings indicate that the FC affects the coaxiality when $b=0.2$ and 0.4 and that the FC has no effect on the co-axiality when $b=0, 0.6, 0.8$ and 1.

3.2 Contributions of contact types

Because the particles in the specimen of a binary granular mixture ($0\% < FC < 100\%$) include coarse and fine particles, the contacts in the specimen can be categorized as cc, cf and ff contacts. The stress ratio can be written as the sum of three stress ratios:

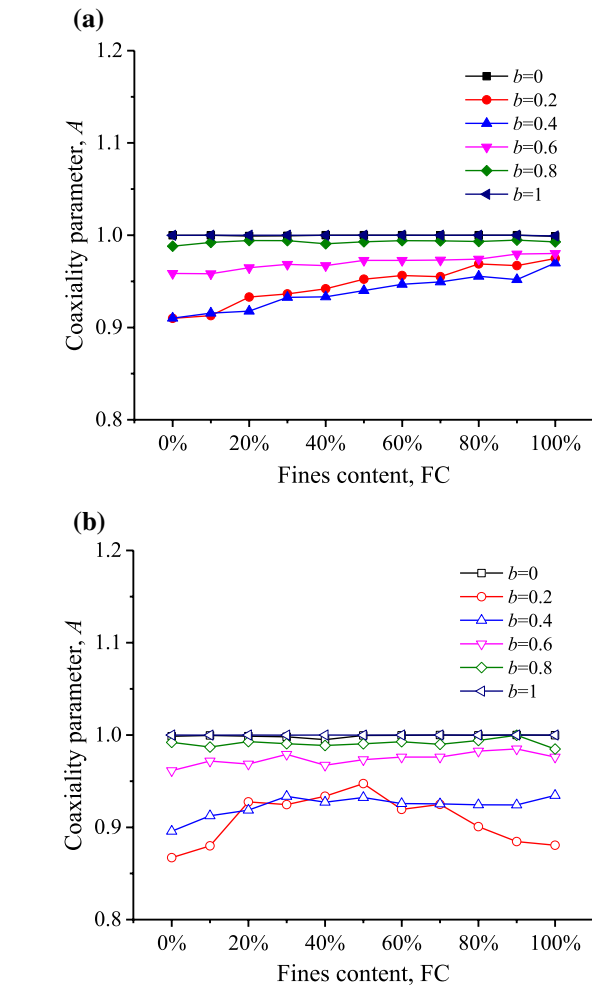


Fig. 14 Variations in the coaxiality parameter with the FC at the a peak and b critical states

$$\frac{q}{p} = \frac{q_{cc}}{p} + \frac{q_{cf}}{p} + \frac{q_{ff}}{p} \tag{13}$$

where q_{cc}, q_{cf} and q_{ff} are the deviatoric stresses of the cc, cf and ff contacts, respectively. Their values can be obtained based on Eqs. (3) and (5) by restricting the cc, cf and ff contacts, respectively. Figure 15 depicts the variations in the stress ratios of the cc, cf and ff contacts q_{sub}/p (q_{sub}/p represents $q_{cc}/p, q_{cf}/p$ and q_{ff}/p) versus the FC. Clearly, the b value influences q_{sub}/p . For a given FC, the three stress ratios generally decrease as the b value increases, which leads to the fact that the stress ratio q/p generally decreases as the b value increases as shown in Fig. 5. The variations in the percentage contributions of the cc, cf and ff contacts to the stress ratio PC_{sub} (PC_{sub} represents PC_{cc}, PC_{cf} and PC_{ff}) with the FC are depicted in Fig. 16. According to Lopez et al. [27], considering the percentage contributions of the cc, cf and ff contacts, the binary granular mixtures can be classified as several types by three thresholds of the FC (i.e., $FC_1,$

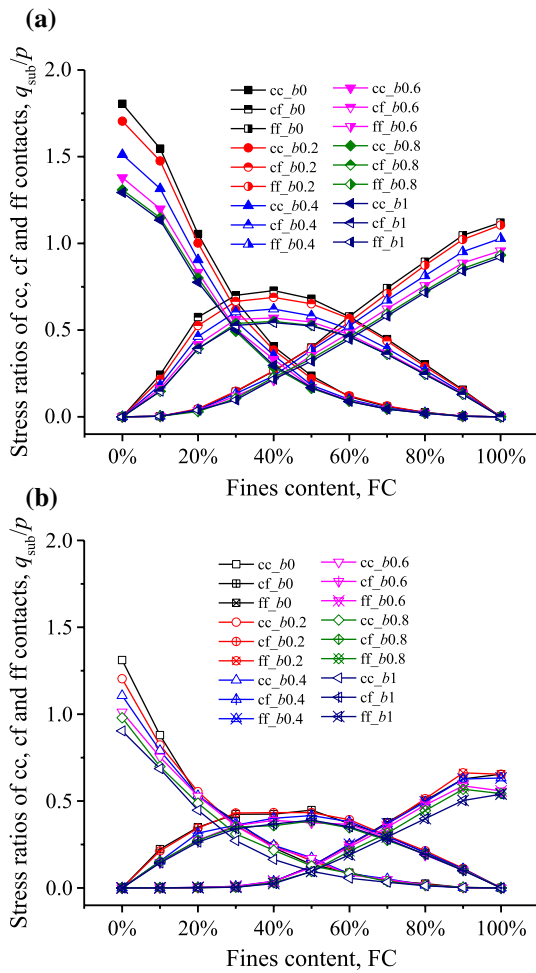


Fig. 15 Variations in the stress ratios of the cc, cf and ff contacts versus the FC at the **a** peak and **b** critical states

FC_2 and FC_3 , as shown in Fig. 16). Specifically, as $FC < FC_1$ ($PC_{cc} > PC_{cf} > PC_{ff}$), the binary granular mixtures are underfilled. As $FC_1 < FC < FC_2$ ($PC_{cf} > PC_{cc} > PC_{ff}$), the binary granular mixtures are interactive-underfilled. As $FC_2 < FC < FC_3$ ($PC_{cf} > PC_{ff} > PC_{cc}$), the binary granular mixtures are interactive-overfilled. As $FC > FC_3$ ($PC_{ff} > PC_{cf} > PC_{cc}$), the binary granular mixtures are overfilled. Interestingly, at both the peak and critical states, the b value has an insignificant influence on the three thresholds of the FC. $FC_1 \approx 30\%$, $FC_2 \approx 44\%$ and $FC_3 \approx 60\%$ at the peak state, while $FC_1 \approx 30\%$, $FC_2 \approx 51\%$ and $FC_3 \approx 68\%$ at the critical state. This finding indicates that the b value generally has no influence on the classification of binary granular mixtures.

The contacts in a specimen can also be categorized as strong and weak contacts. The contact forces of strong contacts are greater than or equals the mean contact force, while the contact forces of weak contacts are less than the

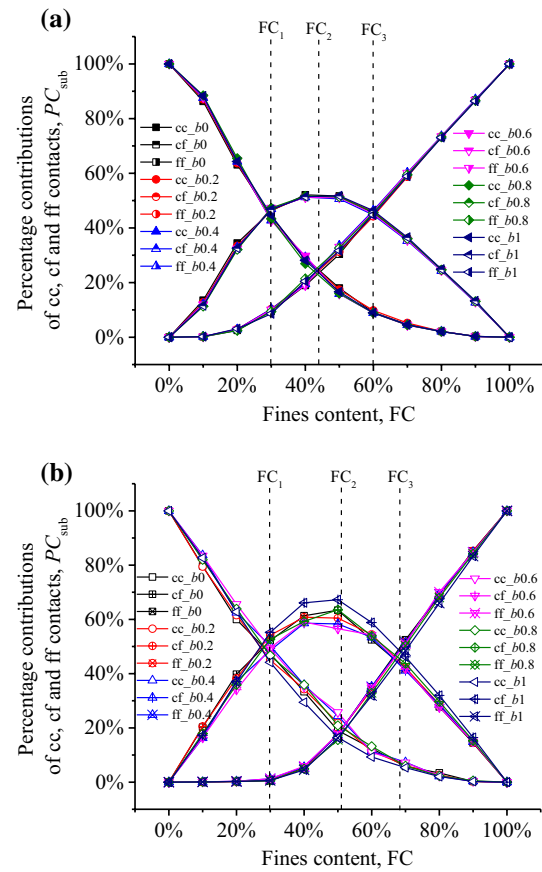


Fig. 16 Variations in the percentage contributions of the cc, cf and ff contacts to the stress ratio with the FC at the **a** peak and **b** critical states

mean contact force [55]. The stress ratio can be written as the sum of two stress ratios:

$$\frac{q}{p} = \frac{q_s}{p} + \frac{q_w}{p} \tag{14}$$

where q_s and q_w are the deviatoric stresses of the strong and weak contacts, respectively. Their values can be calculated based on Eqs. (3) and (5) by restricting strong and weak contacts. Figure 17 depicts the variations in the stress ratios of strong and weak contacts q_{sub}/p (q_{sub}/p represents q_s/p and q_w/p) with the FC. Evidently, the b value influences q_{sub}/p . In Fig. 17a, as regards strong contacts, for a specific FC, as the b value increases, q_s/p decreases. As regards weak contacts, when $FC \leq 10\%$, for a specific FC, as the b value increases, q_w/p roughly decreases. When $FC \geq 20\%$, for a given FC, q_w/p generally increases with increasing b . Figure 17a indicates why q/p varies with the b value in Fig. 5a. When $FC \leq 10\%$, with increasing b , decreases in q_s/p and q_w/p result in a decrease in q/p . When $FC \geq 20\%$, with increasing b , a decrease in q_s/p exceeds an increase

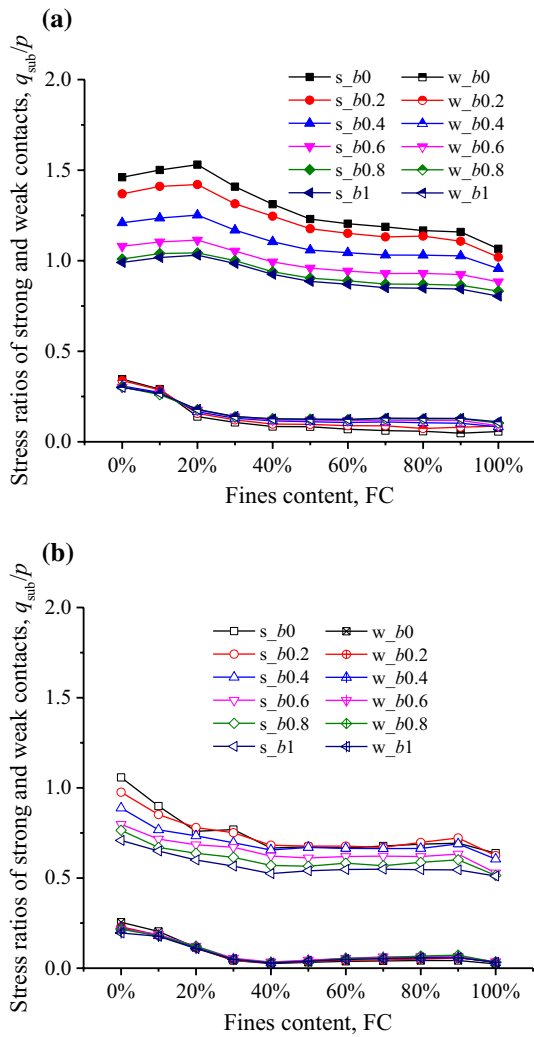


Fig. 17 Variations in the stress ratios of strong and weak contacts with the FC at the **a** peak and **b** critical states

in q_w/p , resulting in a decrease in q/p . In Fig. 17b, as regards strong contacts, for a given FC, with increasing b , q_s/p roughly decreases. As regards weak contacts, q_w/p is roughly unaffected by the b value. Figure 17b manifests why q/p varies with the b value in Fig. 5b. For a given FC, with increasing b , a rough decrease in q_s/p results in a rough decrease in q/p . Figure 18 depicts the variations in the percentage contributions of strong and weak contacts to the stress ratio PC_{sub} (PC_{sub} represents PC_s and PC_w) with the FC. Obviously, PC_s is larger than 75% and PC_w is smaller than 25%, which indicate that the strong contacts are the major contributor to the stress ratio. In addition, the b value influences PC_s and PC_w . For a specific FC, PC_s decreases and PC_w increases with increasing b .

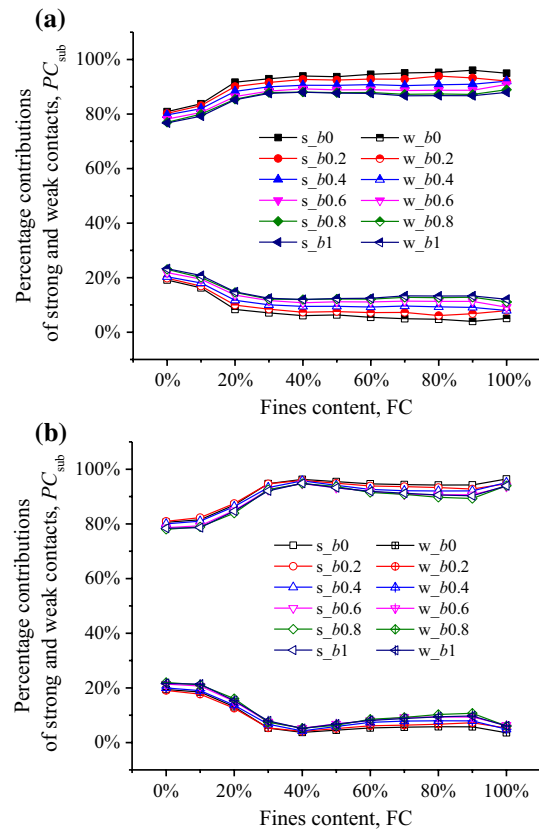


Fig. 18 Variations in the percentage contributions of strong and weak contacts to the stress ratio with the FC at the **a** peak and **b** critical states

3.3 Microscale responses

As suggested by Minh and Cheng [56] and Shire et al. [36], the partial coordination number Z_{cc} for a specimen comprising of spherical coarse and fine particles can be calculated by:

$$Z_{cc} = 2C_{cc}/N_{cp} \tag{15}$$

where C_{cc} is the number of cc contacts and N_{cp} is the number of coarse particles. As indicated in the literature [57–59], the coordination number has two definitions for multisphere particles. One is the average number of particles in contact with a particle, and the other is the number of contacts between subspheres constituting various multisphere particles divided by the number of multisphere particles. Because every irregular coarse particle consists of overlapping subspheres, the partial coordination number of binary granular mixtures in this study also has two definitions similar to those of the coordination number, as follows:

$$Z_{cc}^{pp} = 2C_{cc}^{pp}/N_{cp} \tag{16}$$

$$Z_{cc}^{ss} = 2C_{cc}^{ss}/N_{cp} \tag{17}$$

where Z_{cc}^{pp} is the partial coordination number based on the “particle–particle” approach; C_{cc}^{pp} is the number of contacts between various multisphere coarse particles (not between subspheres); Z_{cc}^{ss} is the partial coordination number based on the “subsphere–subsphere” approach; and C_{cc}^{ss} is the number of contacts between subspheres constituting various multisphere coarse particles.

Figure 19 depicts the variations in the partial coordination number based on the “particle–particle” approach Z_{cc}^{pp} versus the FC. Z_{cc}^{pp} gradually decreases with increasing FC at the peak and critical states because the coarse particles are gradually separated by the fine particles. However, it was observed that the b value has an insignificant effect on Z_{cc}^{pp} . As indicated in Fig. 16, when binary granular mixtures change from an underfilled structure to an interactive-underfilled structure at the peak and critical states, $FC_1 \approx 30\%$. Figure 20 depicts the probability distributions of the number of coarse particles in contact with a coarse particle N^{cc} for

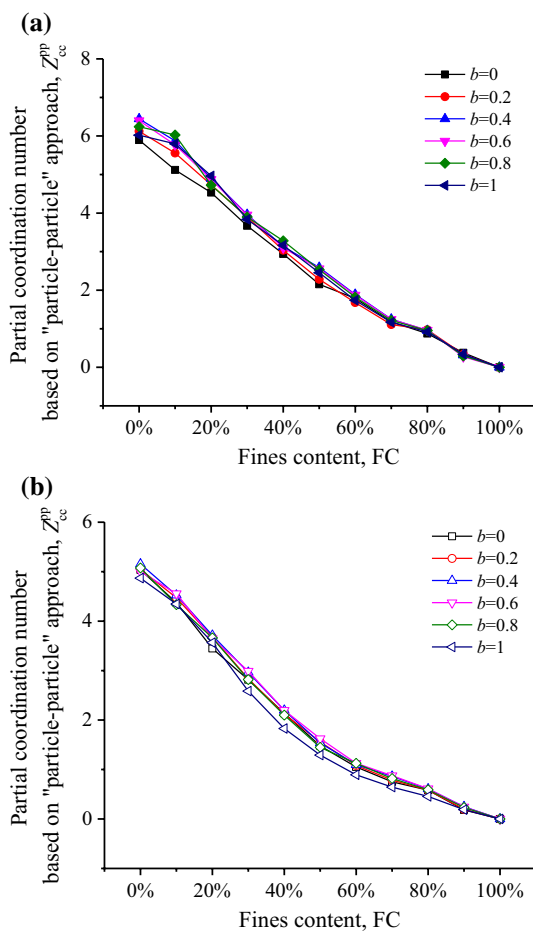


Fig. 19 Variations in the partial coordination number based on the “particle–particle” approach versus the FC at the **a** peak and **b** critical states

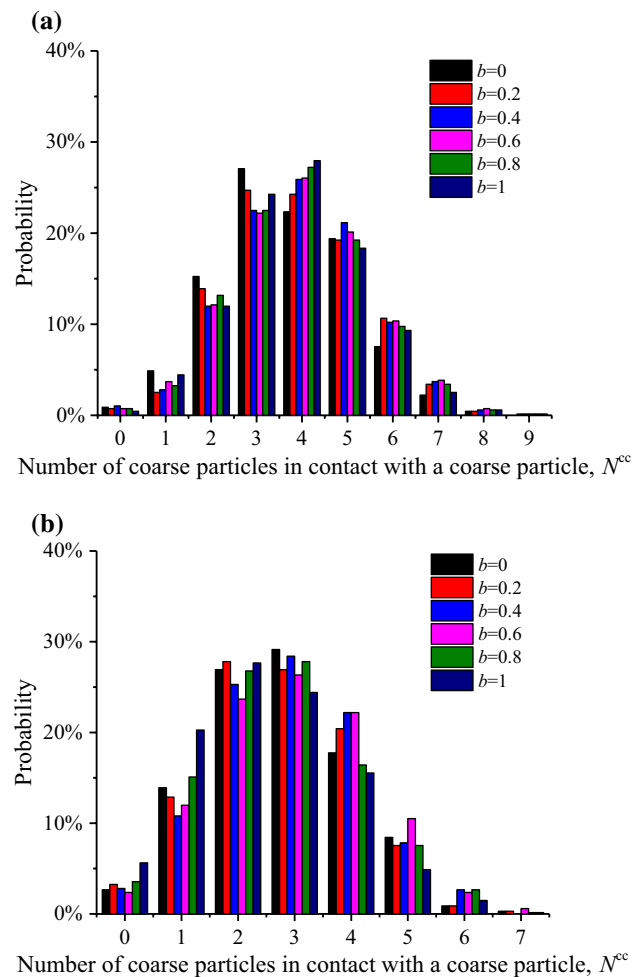


Fig. 20 Probability distributions of the number of coarse particles in contact with a coarse particle for $FC = 30\%$ at the **a** peak and **b** critical states

$FC = 30\%$. Obviously, these probability distributions show unimodal characteristics. At the peak state, the probabilities of $N^{cc}=3$ and $N^{cc}=4$ are the largest, around 25%, followed by that of $N^{cc}=5$, around 20%. At the critical state, the probabilities of $N^{cc}=2$ and $N^{cc}=3$ are the largest, around 25%, followed by those of $N^{cc}=1$ and $N^{cc}=4$.

Figure 21 depicts the variations in the partial coordination number based on the “subsphere–subsphere” approach Z_{cc}^{ss} versus the FC. Interestingly, the b value influences Z_{cc}^{ss} . Specifically, at the peak state, for a given FC, an increase in the b value leads to an increase in Z_{cc}^{ss} when $FC \leq 60\%$, which indicates that the interlocking between coarse particles is enhanced. At the critical state, for a given FC, with increasing b , Z_{cc}^{ss} first increases and then decreases when $FC \leq 60\%$, which indicates that the interlocking between coarse particles is first strengthened and then weakened. At both the peak and critical states, the b value almost has no effect on Z_{cc}^{ss} when $FC > 60\%$, which can be ascribed to the truth that

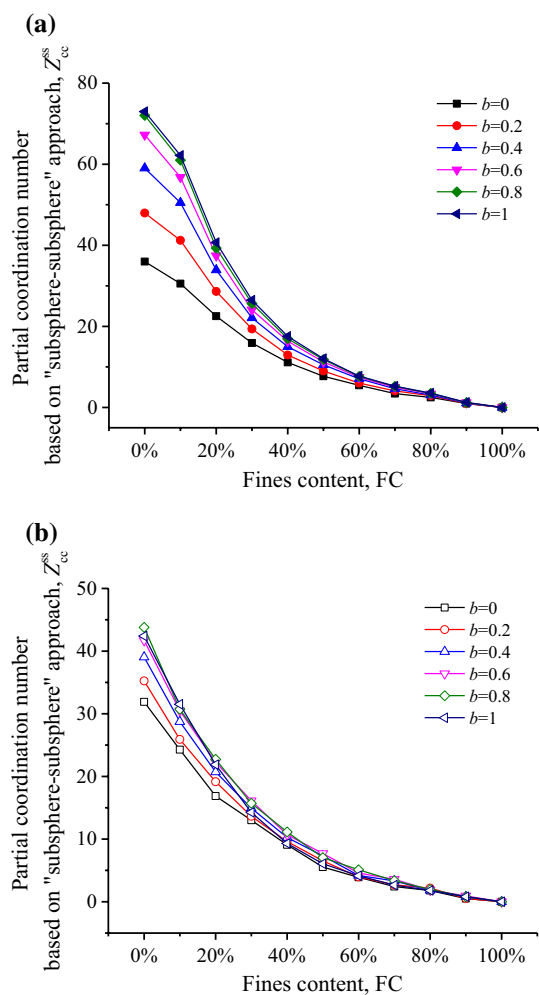


Fig. 21 Variations in the partial coordination number based on the “subsphere–subsphere” approach versus the FC at the **a** peak and **b** critical states

the coarse particles are suspended in the fine particle matrix when $FC > 60\%$. Figure 22 depicts the relationship between the relative peak dilatancy angle ψ_p/ψ_{p100} and the difference between the partial coordination numbers based on the “subsphere–subsphere” approach at the peak and critical states $(Z_{cc}^{ss})_p - (Z_{cc}^{ss})_c$, where ψ_{p100} is the peak dilatancy angle of the binary granular mixture with $FC = 100\%$, having the same b value with ψ_p . Clearly, the data can be fitted by $\psi_p/\psi_{p100} = 0.0395[(Z_{cc}^{ss})_p - (Z_{cc}^{ss})_c] + 1.007$. This finding means that the peak dilatancy angle is related to the partial coordination number based on the “subsphere–subsphere” approach for a binary granular mixture.

In three dimensions, the rotation of each particle is a vector which has three components about the x , y and z axes. In this study, the magnitude of the vector, called a rotation angle, was used. Figure 23 shows the variations in the average rotation angles of coarse and fine particles

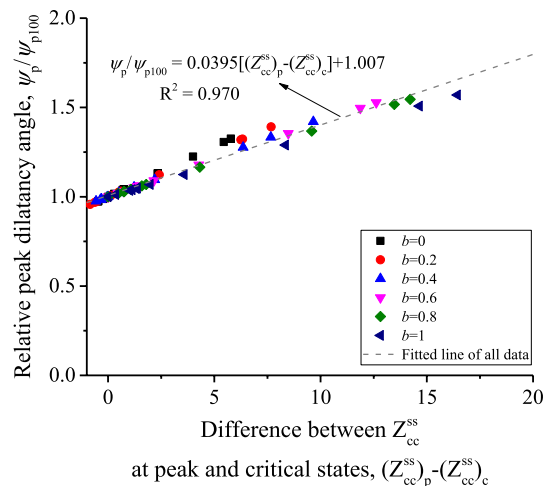


Fig. 22 Relationship between the relative peak dilatancy angle and the difference between the partial coordination numbers based on the “subsphere–subsphere” approach at the peak and critical states

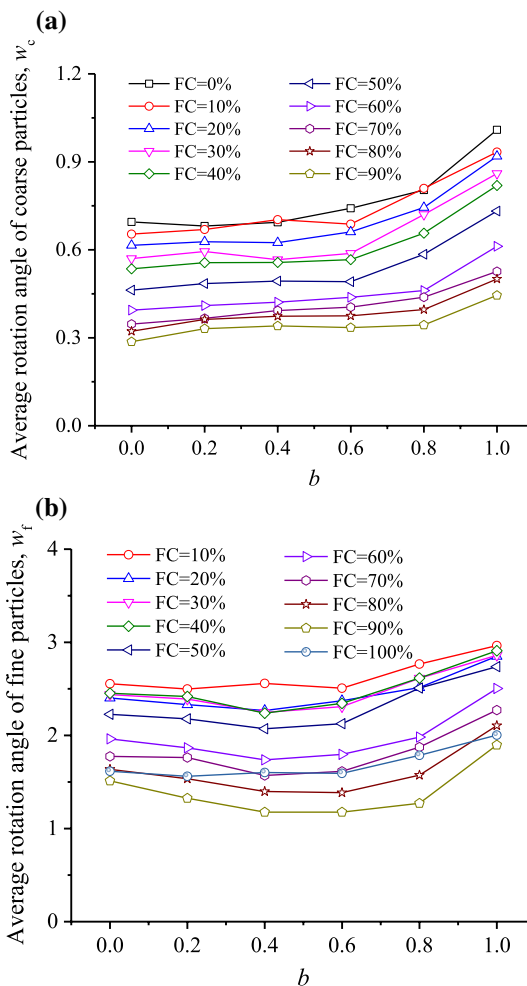


Fig. 23 Variations in the average rotation angles of **a** coarse and **b** fine particles with the b value at the axial strain of 40%

(i.e., w_c and w_f) with the b value at the axial strain of 40%. Obviously, for a binary granular mixture with a specific FC ($0\% < FC < 100\%$) and b value, w_f is larger than w_c . The result means that spherical fine particles play a major role in harmonizing the deformation of a specimen, while irregular coarse particles play a minor role. Furthermore, for a given b value, with increasing FC ($FC < 100\%$), w_c and w_f generally decrease.

3.4 Anisotropies of contacts and contact forces

Oda [60] and Satake [61] suggested a quantity to measure the fabric anisotropy, which is expressed as:

$$\phi_{ij} = \int_{\Omega} E(\mathbf{n}) n_i n_j d\mathbf{n} = \frac{1}{C} \sum n_i n_j \tag{18}$$

where \mathbf{n} denotes a unit vector along a direction; n_i and n_j are the i th component and the j th component of \mathbf{n} , respectively; Ω represents all possible contact directions; $E(\mathbf{n})$ denotes the probability density of the directions of the contacts; C is the number of contacts. $E(\mathbf{n})$ is written as [62]:

$$E(\mathbf{n}) = \frac{1}{4\pi} (1 + a_{ij}^c n_i n_j) \tag{19}$$

where a_{ij}^c is the tensor to describe the directional distribution of contacts and is deduced as [63]:

$$a_{ij}^c = \frac{15}{2} \phi'_{ij} \tag{20}$$

where ϕ'_{ij} denotes the deviatoric tensor of ϕ_{ij} . Contact forces can be divided into the normal contact forces and the tangential contact forces, whose anisotropies can be quantified as [41]:

$$F_{ij}^n = \frac{1}{4\pi} \int_{\Omega} \bar{f}^n(\mathbf{n}) n_i n_j d\mathbf{n} = \sum \frac{f_n n_i n_j}{C(1 + a_{kl}^c n_k n_l)} \tag{21}$$

$$F_{ij}^t = \frac{1}{4\pi} \int_{\Omega} \bar{f}^t(\mathbf{n}) t_i n_j d\mathbf{n} = \sum \frac{f_t t_i n_j}{C(1 + a_{kl}^c n_k n_l)} \tag{22}$$

$$\bar{f}^n(\mathbf{n}) = \bar{f}_0 (1 + a_{ij}^n n_i n_j) \tag{23}$$

$$\bar{f}_i^t(\mathbf{n}) = \bar{f}_0 (a_{ij}^t n_j - (a_{kl}^t n_k n_l) n_i) \tag{24}$$

where a_{ij}^n and a_{ij}^t are the tensors to describe the distributions of the directions of normal and tangential contact forces, respectively. They are determined by:

$$a_{ij}^n = \frac{15F_{ij}^{n'}}{2\bar{f}_0} \quad a_{ij}^t = \frac{15F_{ij}^{t'}}{3\bar{f}_0} \quad \bar{f}_0 = F_{ii}^n \tag{25}$$

where $F_{ij}^{n'}$ and $F_{ij}^{t'}$ are the deviatoric parts of F_{ij}^n and F_{ij}^t , respectively. The scalar a_* is used to quantify the degrees of the anisotropies of contacts and contact forces:

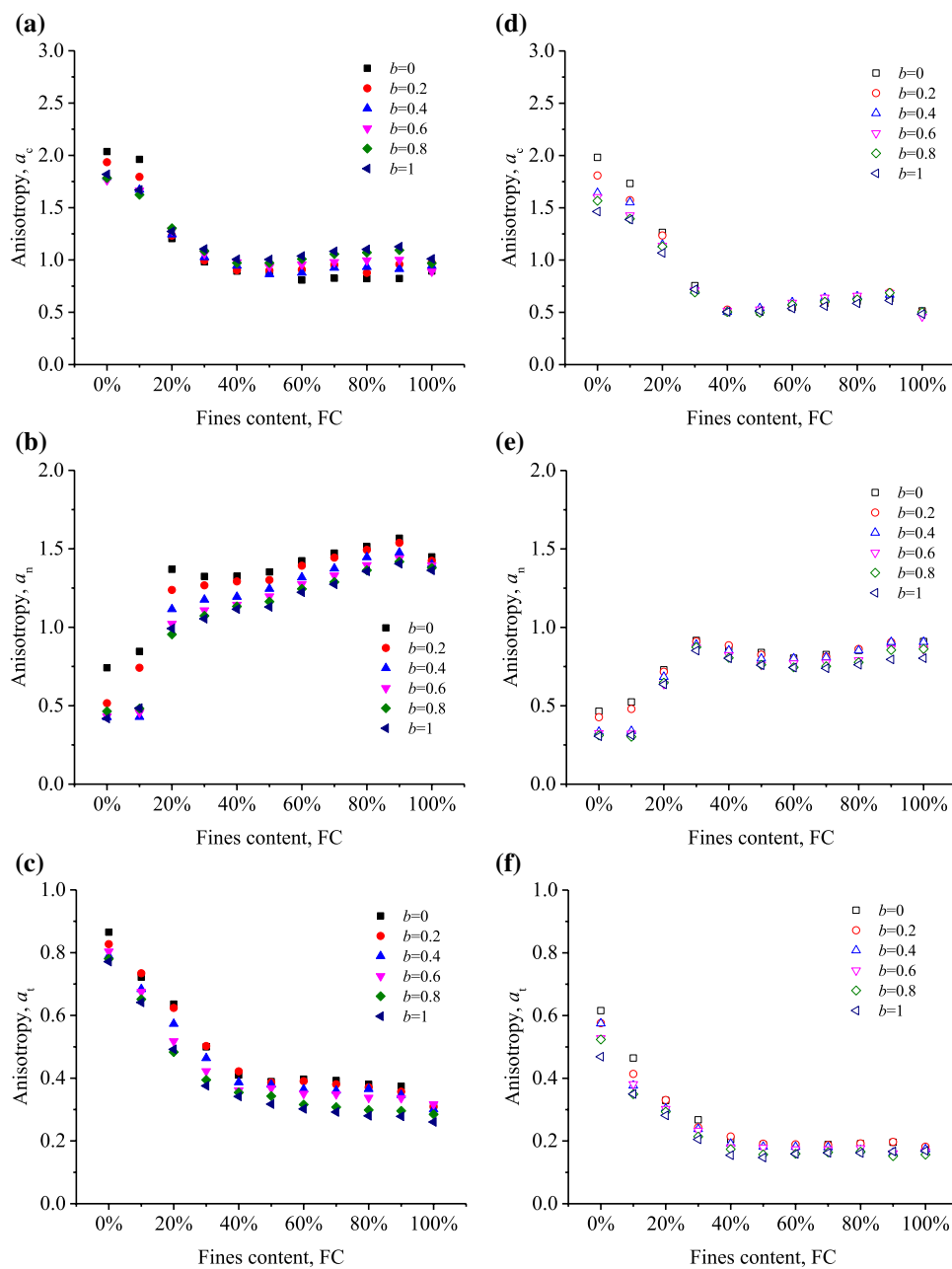
$$a_* = \text{sign}(S_r) \sqrt{\frac{3}{2} a_*^* a_*^*} \tag{26}$$

where a_* represents the anisotropy of contacts a_c , the anisotropy of normal contact forces a_n and the anisotropy of tangential contact forces a_t ; S_r represents a normalized scalar of the product of a_{ij}^* and σ'_{ij} [41].

During the true triaxial compression test, the contacts, contact forces and branch vectors in a specimen are anisotropic. Note that the anisotropies of contacts, contact forces and branch vectors can be used to describe the microscale mechanisms of the stress ratio q/p when the specimen is subjected to axisymmetric loading (i.e., $b=0$); that is, the stress ratio approaches to the sum of the anisotropies of contacts, contact forces and branch vectors [41]. According to the previous studies [18, 64] investigating the shear behaviors of specimens composed of spherical particles, when $b \neq 0$, the stress–force–fabric relationship is not accurate enough. Nevertheless, to some extent, the anisotropies can help us to further understand the microscale mechanisms of the stress ratio changing with the b value for binary granular mixtures with various FCs. In addition, compared with the anisotropies of contacts and contact forces, the anisotropy of branch vectors is very small. Thus, this study mainly focused on the anisotropies of the contacts and contact forces.

Figures 24a–c illustrate the anisotropies at the peak state. In Fig. 24a, when $FC \leq 10\%$, a_c generally decreases with increasing b . However, when $FC \geq 40\%$, a_c generally increases with increasing b , consistent with the result obtained by Zhou et al. [18], who investigated the effect of the b value on the shear behaviors of spheres with a narrow gradation. In Fig. 24b, a_n basically decreases with increasing b . In Fig. 24c, with increasing b , a_t generally decreases. To some extent, a combination of Fig. 24a–c manifests the microscale mechanisms of the dependence of the stress ratio q/p on the b value at the peak state as shown in Fig. 5a. When $FC \leq 10\%$, with increasing b , decreases in a_c , a_n and a_t result in a decrease in q/p . When $20\% \leq FC \leq 30\%$, with increasing b , decreases in both a_n and a_t lead to a decrease in q/p . When $FC \geq 40\%$, with increasing b , the sum of decreases in both a_n and a_t exceeds an increase in a_c , causing a decrease in q/p . Figure 24d–f illustrate the anisotropies at the critical state. In Fig. 24d, when $FC \leq 20\%$, a_c generally decreases with increasing b . However, when $FC \geq 30\%$, a_c is generally independent of the b value. In Fig. 24e, a_n basically decreases with increasing b . In Fig. 24f, a_t basically

Fig. 24 Anisotropies at the (a–c) peak and (d–f) critical states



decreases with increasing b . To some extent, a combination of Fig. 24d–f makes us seize the microscale mechanisms of the dependence of the stress ratio q/p on the b value at the critical state as shown in Fig. 5b. When $FC \leq 20\%$, with increasing b , a decrease in q/p can be attributed to the decreases in a_c , a_n and a_t . When $FC \geq 30\%$, with increasing b , decreases in both a_n and a_t result in a decrease in q/p .

4 Conclusions

The effect of the b value on the shear responses of binary granular mixtures with various FCs was investigated via the DEM numerical simulations of true triaxial compression tests. The binary granular mixtures were composed of

coarse particles with real gravel shapes and fine particles with sphere shapes, and the ratio of the coarse particle size to the fine particle size is 4.45. The FC ranges from 0 to 100% in intervals of 10%. The main findings are summarized as follows.

For a specific FC, as the b value increases, both ϕ_p and ϕ_c first increase to a crest and then decrease. For a specific FC, as the b value increases, ψ_p roughly linearly increases. It was found that the shapes of coarse particles play an important role in the peak and critical friction angles and the peak dilatancy angles of binary granular mixtures.

For binary granular mixtures with different FCs and an identical b value, a linear relationship between the peak friction angle (or the peak dilatancy angle) and the change in the void ratio was found. Additionally, an acceptable equation was proposed to predict the peak dilatancy angle of a binary granular mixture. The FC affects the coaxiality when $b=0.2$ and 0.4 and the FC has no effect on the coaxiality when $b=0, 0.6, 0.8$ and 1 . Specifically, at the peak state, with increasing FC, for $b=0.2$ and 0.4 , the coaxiality parameter A increases. At the critical state, with increasing FC, for $b=0.2$, A first increases and then decreases; for $b=0.4$, A increases.

The b value has an insignificant influence on Z_{cc}^{PP} . At the peak state, an increase in the b value leads to an increase in Z_{cc}^{SS} when $FC \leq 60\%$, indicating that the interlocking between coarse particles is enhanced. At the critical state, Z_{cc}^{SS} first increases and then decreases with increasing b when $FC \leq 60\%$, indicating that the interlocking between coarse particles is first strengthened and then weakened. Interestingly, there is a linear relationship between the relative peak dilatancy angle and the difference between the partial coordination numbers based on the “subsphere–subsphere” approach at the peak and critical states.

It was found that the b value generally has no influence on the classification of binary granular mixtures at both the peak and critical states by examining the percentage contributions of cc, cf and ff contacts. The analyses of q_{cc}/p , q_{cf}/p , q_{ff}/p , q_s/p and q_w/p indicate why q/p varies with the b value. To some extent, the examination of anisotropies helps us to further understand the microscale mechanisms that underly the dependence of q/p on the b value.

Acknowledgments The authors are grateful for the financial support given by these projects, including the Fundamental Research Funds for the Central Universities of Central South University (No. 2018zzts195) and the National Natural Science Foundation of China (No. 51809292). The authors thank Prof. Nie (Zhihong Nie) for his help in the initial stage of the paper.

Author contributions Xiaoping Cao: conceptualization, investigation, validation, visualization, data curation. Yangui Zhu: formal analysis, writing-original draft, writing- reviewing and editing, funding acquisition, supervision, project administration. Jian Gong: methodology, software, funding acquisition, resources.

Declarations

Conflict of interest The authors declare no conflict of interest.

References

1. Kumruzzaman, M., Yin, J.-H.: Influences of principal stress direction and intermediate principal stress on the stress–strain–strength behaviour of completely decomposed granite. *Can. Geotech. J.* **47**(2), 164–179 (2010)
2. Kumruzzaman, M., Yin, J.H.: Influence of the intermediate principal stress on the stress–strain–strength behaviour of a completely decomposed granite soil. *Geotechnique* **62**(3), 275–280 (2012)
3. Xiao, Y., Liu, H., Chen, Y., Chu, J.: Influence of intermediate principal stress on the strength and dilatancy behavior of rockfill material. *J. Geotech. Geoenviron. Eng.* **140**(11), 04014064 (2014)
4. Kandasami, R.K., Murthy, T.G.: Experimental studies on the influence of intermediate principal stress and inclination on the mechanical behaviour of angular sands. *Granul. Matter* **17**(2), 217–230 (2015)
5. Xiao, Y., Sun, Y., Liu, H., Yin, F.: Critical state behaviors of a coarse granular soil under generalized stress conditions. *Granul. Matter* **18**(2), 17 (2016)
6. Kandasami, R.K., Murthy, T.G.: Manifestation of particle morphology on the mechanical behaviour of granular ensembles. *Granul. Matter* **19**(2), 21 (2017)
7. Qu, T., Feng, Y.T., Wang, Y., Wang, M.: Discrete element modelling of flexible membrane boundaries for triaxial tests. *Comput. Geotech.* **115**, 103154 (2019)
8. Barnett, N., Rahman, M.M., Karim, M.R., Nguyen, H.B.K.: Evaluating the particle rolling effect on the characteristic features of granular material under the critical state soil mechanics framework. *Granul. Matter* **22**(4) (2020)
9. Ng, T.-T., Ge, L.: Packing void ratios of very dense ternary mixtures of similar ellipsoids. *Granul. Matter* **22**(2) (2020)
10. Ng, T.T.: Shear strength of assemblies of ellipsoidal particles. *Geotechnique* **54**(10), 659–669 (2004)
11. Barreto, D., O’Sullivan, C.: The influence of inter-particle friction and the intermediate stress ratio on soil response under generalised stress conditions. *Granul. Matter* **14**(4), 505–521 (2012)
12. Sazzad, M.M., Suzuki, K., Modaressi-Farahmand-Razavi, A.: Macro-micro responses of granular materials under different b values using DEM. *Int. J. Geomech.* **12**(3), 220–228 (2012)
13. O’Sullivan, C., Wadee, M.A., Hanley, K.J., Barreto, D.: Use of DEM and elastic stability analysis to explain the influence of the intermediate principal stress on shear strength. *Geotechnique* **63**(15), 1298–1309 (2013)
14. Sazzad, M.M., Suzuki, K.: Density dependent macro-micro behavior of granular materials in general triaxial loading for varying intermediate principal stress using DEM. *Granul. Matter* **15**(5), 583–593 (2013)
15. Huang, X., Hanley, K.J., O’Sullivan, C., Kwok, C.Y., Wadee, M.A.: DEM analysis of the influence of the intermediate stress ratio on the critical-state behaviour of granular materials. *Granul. Matter* **16**(5), 641–655 (2014)
16. Li, B., Zhang, F., Gutierrez, M.: A numerical examination of the hollow cylindrical torsional shear test using DEM. *Acta Geotech.* **10**(4), 449–467 (2014)
17. Li, B., Chen, L., Gutierrez, M.: Influence of the intermediate principal stress and principal stress direction on the mechanical behavior of cohesionless soils using the discrete element method. *Comput. Geotech.* **86**, 52–66 (2017)

18. Zhou, W., Liu, J., Ma, G., Chang, X.: Three-dimensional DEM investigation of critical state and dilatancy behaviors of granular materials. *Acta Geotech.* **12**(3), 527–540 (2017)
19. Vallejo, L.E., Mawby, R.: Porosity influence on the shear strength of granular material-clay mixtures. *Eng. Geol.* **58**(2), 125–136 (2000)
20. Vallejo, L.E.: Interpretation of the limits in shear strength in binary granular mixtures. *Can. Geotech. J.* **38**(5), 1097–1104 (2001)
21. Gong, J., Nie, Z., Zhu, Y., Liang, Z., Wang, X.: Exploring the effects of particle shape and content of fines on the shear behavior of sand-fines mixtures via the DEM. *Comput. Geotech.* **106**, 161–176 (2019)
22. Ng, T.T., Zhou, W., Chang, X.L.: Effect of particle shape and fine content on the behavior of binary mixture. *J. Eng. Mech.* **143**(1), 9 (2016)
23. Gong, J., Liu, J.: Mechanical transitional behavior of binary mixtures via DEM: Effect of differences in contact-type friction coefficients. *Comput. Geotech.* **85**, 1–14 (2017)
24. Gong, J., Liu, J., Cui, L.: Shear behaviors of granular mixtures of gravel-shaped coarse and spherical fine particles investigated via discrete element method. *Powder Technol.* **353**, 178–194 (2019)
25. Xiao, Y., Long, L., Evans, T.M., Zhou, H., Liu, H., Stuedlein, A.W.: Effect of particle shape on stress-dilatancy responses of medium-dense sands. *J. Geotech. Geoenviron. Eng.* **145**(2), 04018105 (2019)
26. Xiao, Y., Stuedlein, A.W., Ran, J., Evans, T.M., Cheng, L., Liu, H., van Paassen, L.A., Chu, J.: Effect of particle shape on strength and stiffness of biocemented glass beads. *J. Geotech. Geoenviron. Eng.* **145**(11), 06019016 (2019)
27. Lopez, R.D., Silfwerbrand, J., Jelagin, D., Birgisson, B.: Force transmission and soil fabric of binary granular mixtures. *Geotechnique* **66**(7), 578–583 (2016)
28. ICOLD: Bulletin 164: Internal Erosion of Dams, Dikes, and their Foundations. Paris, France. (2013)
29. Itasca: User's Manual for PFC3D version PFC5.0. Itasca Consulting Group Inc., Minneapolis (2014)
30. Taghavi, R.: Automatic clump generation based on mid-surface. In: *Proceedings of the Continuum and Distinct Element Numerical Modeling In Geomechanics* (2011)
31. Salgado, R., Bandini, P., Karim, A.: Shear strength and stiffness of silty sand. *J. Geotech. Geoenviron. Eng.* **126**(5), 451–462 (2000)
32. Lee, J., Salgado, R., Carraro, J.A.H.: Stiffness degradation and shear strength of silty sands. *Can. Geotech. J.* **41**(5), 831–843 (2004)
33. Carraro, J.A.H., Prezzi, M., Salgado, R.: Shear strength and stiffness of sands containing plastic or nonplastic fines. *J. Geotech. Geoenviron. Eng.* **135**(9), 1167–1178 (2009)
34. Lopez, R.D., Ekblad, J., Silfwerbrand, J.: Resilient properties of binary granular mixtures: A numerical investigation. *Comput. Geotech.* **76**, 222–233 (2016)
35. Lade, P.V., Liggio, C.D., Yamamuro, J.A.: Effect of nonplastic fines on minimum and maximum void ratios of sand. *Geotech. Test. J.* **21**(4), 336–347 (1998)
36. Shire, T., O'Sullivan, C., Hanley, K.J.: The influence of fines content and size-ratio on the micro-scale properties of dense bimodal materials. *Granul. Matter* **18**(3), 52 (2016)
37. Horn, H.M., Deere, D.U.: Frictional characteristics of minerals. *Geotechnique* **12**(4), 319–335 (1962)
38. Rowe, P.W.: Stress-dilatancy relation for static equilibrium of an assembly of particles in contact. In: *Proceedings of the Royal Society A: Mathematical, Physical and Engineering Sciences* (1962)
39. Senetakis, K., Coop, M.R., Todisco, M.C.: The inter-particle coefficient of friction at the contacts of Leighton Buzzard sand quartz minerals. *Soils Found.* **53**(5), 746–755 (2013)
40. Senetakis, K., Coop, M.R., Todisco, M.C.: Tangential load–deflection behaviour at the contacts of soil particles. *Geotech. Lett.* **3**(2), 59–66 (2013)
41. Guo, N., Zhao, J.: The signature of shear-induced anisotropy in granular media. *Comput. Geotech.* **47**, 1–15 (2013)
42. Guo, N., Zhao, J.: Local fluctuations and spatial correlations in granular flows under constant-volume quasistatic shear. *Phys. Rev. E* **89**(4), 042208 (2014)
43. Gu, X.Q., Huang, M.S., Qian, J.G.: DEM investigation on the evolution of microstructure in granular soils under shearing. *Granul. Matter* **16**(1), 91–106 (2014)
44. Coetzee, C.J.: Calibration of the discrete element method and the effect of particle shape. *Powder Technol.* **297**, 50–70 (2016)
45. Goldenberg, C., Goldhirsch, I.: Friction enhances elasticity in granular solids. *Nature* **435**(7039), 188–191 (2005)
46. Jiang, M., Shen, Z., Wang, J.: A novel three-dimensional contact model for granulates incorporating rolling and twisting resistances. *Comput. Geotech.* **65**, 147–163 (2015)
47. da Cruz, F., Emam, S., Prochnow, M., Roux, J.N., Chevoir, F.: Rheophysics of dense granular materials: Discrete simulation of plane shear flows. *Phys. Rev. E* **72**(2), 021309 (2005)
48. Perez, J.C.L., Kwok, C.Y., O'Sullivan, C., Huang, X., Hanley, K.J.: Assessing the quasi-static conditions for shearing in granular media within the critical state soil mechanics framework. *Soils Found.* **56**(1), 152–159 (2016)
49. Christoffersen, J., Mehrabadi, M.M., Nemat-Nasser, S.: A micro-mechanical description of granular material behavior. *J. Appl. Mech.* **48**(2), 339–344 (1981)
50. Schanz, T., Vermeer, P.A.: Angles of friction and dilatancy of sand. *Geotechnique* **46**(1), 145–151 (1996)
51. Nie, Z., Fang, C., Gong, J., Liang, Z.: DEM study on the effect of roundness on the shear behaviour of granular materials. *Comput. Geotech.* **121**, 103457 (2020)
52. Jamiolkowski, M., Kongsukprasert, L., Lo Presti, D.: Characterization of gravelly geomaterials. In: *Proceedings of the Fifth International Geotechnical Conference, Bangkok, Thailand* (2004)
53. Zhao, J., Guo, N.: Unique critical state characteristics in granular media considering fabric anisotropy. *Geotechnique* **63**(8), 695–704 (2013)
54. Zhou, W., Wu, W., Ma, G., Ng, T.-T., Chang, X.: Undrained behavior of binary granular mixtures with different fines contents. *Powder Technol.* **340**, 139–153 (2018)
55. Radjai, F., Wolf, D.E., Jean, M., Moreau, J.J.: Bimodal character of stress transmission in granular packings. *Phys. Rev. Lett.* **80**(1), 61–64 (1998)
56. Minh, N.H., Cheng, Y.P.: A DEM investigation of the effect of particle-size distribution on one-dimensional compression. *Geotechnique* **63**(1), 44–53 (2013)
57. Markauskas, D., Kacianauskas, R., Dziugys, A., Navakas, R.: Investigation of adequacy of multi-sphere approximation of elliptical particles for DEM simulations. *Granul. Matter* **12**(1), 107–123 (2010)
58. Azema, E., Radjai, F., Saint-Cyr, B., Delenne, J.Y., Sornay, P.: Rheology of three-dimensional packings of aggregates: Microstructure and effects of nonconvexity. *Phys. Rev. E* **87**(5), 052205 (2013)
59. Nie, Z., Zhu, Y., Wang, X., Gong, J.: Investigating the effects of Fourier-based particle shape on the shear behaviors of rockfill material via DEM. *Granul. Matter* **21**(2), 22 (2019)
60. Oda, M.: Fabric tensor for discontinuous geological materials. *Soils Found.* **22**(4), 96–108 (1982)
61. Satake, M.: Fabric tensor in granular materials. In: *Proceedings of the IUTAM Symposium on Deformation and Failure of Granular Materials, Delft* (1982)
62. Oudafel, H., Rothenburg, L.: 'Stress–force–fabric' relationship for assemblies of ellipsoids. *Mech. Mater.* **33**, 201–221 (2001)

63. Kanatani, K.I.: Distribution of directional data and fabric tensors. *Int. J. Eng. Sci.* **22**(2), 149–164 (1984)
64. Foroutan, T., Mirghasemi, A.A.: CFD-DEM model to assess stress-induced anisotropy in undrained granular material. *Comput. Geotech.* **119**, 103318 (2020)

Publisher's Note Springer Nature remains neutral with regard to jurisdictional claims in published maps and institutional affiliations.